Bias Dependence of High-Frequency Noise in Heterojunction Bipolar Transistors

Mirza M. Jahan, Kuo-Wei Liu, and A. F. M. Anwar, *Senior Member, IEEE*

***Abstract*—Hawkins' isothermal model developed to study noise in bipolar junction transistors (BJTs) is modified to investigate bias-dependent noise in heterojunction bipolar transistors (HBTs) by incorporating thermal effects. It is shown that the inclusion of thermal effects into the high-frequency noise model of HBTs is necessary as the temeperature of the device may become very different from the ambient temperature, especially at high bias current. Calculation of the noise figure by including the thermal effect shows that the isothermal calculation may underestimate the noise figure at high bias current. It is observed that noise at low bias is ideality factor n dependent whereas high bias noise is insensitive to the variation of n. Moreover, the common base current gain plays a major role in the calculation of the minimum noise figure. The excellent fit obtained between the theoretical calculation and the measured data are attributed to the inclusion of the bias-dependent junction heating as well as $C_{\rm De}$ and $C_{\rm bc}$ into the present calculation.**

***Index Terms*—Heterojunction bipolar transistor (HBT), high-frequency noise, thermal effects.**

I. Introduction

THE most widely used noise model for bipolar junction transistors (BJTs) is credited to Hawkins [1]. The model has been quite successful in explaining the high-frequency noise performance of BJTs. Presently, the same model has been adopted to study the bias-dependent noise performance of heterojunction bipolar transistors (HBTs) at high frequency [2], [3]. Escotte *et al*. [4] report a high-frequency model valid for HBTs operating at low bias with model parameters extracted from experimental data. It has been observed, however, that the use of Hawkins' model fails to explain the noise performance of HBTs at higher collector current and at high frequency [3]. The inability of the Hawkins' model, used under isothermal approximation (i.e., junction temperature $\sim$ ambient temperature) to explain the bias dependence of HBT noise performance can be traced to the noninclusion of bias-dependent junction heating effect. As HBTs, unlike BJTs, are operated at higher current density (e.g., 10^5 A/cm^2) and fabricated with compound semiconductor materials with inferior thermal conductivity, junction heating may often lead to poorer noise performance than that predicted by Hawkins' isothermal model.

For silicon-based BJTs, the junction heating effect is not as severe as that in III–V HBTs since silicon has excellent thermal conductivity. The issue of thermal effects is rather serious for compund semiconductors due to their poor thermal conductivity. Consequently, Gao [5] has shown the importance of the inclusion of thermal effects in the analysis of compound semiconductor devices. Kim *et al.* [6] reported the temperature distribution in multifinger HBTs by solving the three-dimensional (3-D) Laplace's equation. The analysis of Liou [7] shows that the current gain fall-off will occur at a much lower current level if thermal effects are included. This is due to the fact that the high device temperature would cease the transistor action by virtually shortening the emitter to the collector. As such, the resistance of the base region will also deteriorate due to increased lattice scattering.

As an HBT is a high current device, the inclusion of the bias dependence of the transistor parameters into the noise model becomes all the more important. This warrants the incorporation of the bias-dependent element like diffusion capacitance $C_{\rm De}$ [8] and base–collector depletion capacitance $C_{\rm bc}$ [8] into the existing Hawkins' model. Moreover, high and low injection effects should also be included. Depending on the injection level (high, low, or medium), common base current gain α_0, base transit time t_b, and base–emitter junction ideality factor n may vary. In addition, due to the effective increase of the base width at high bias current, t_b be comes greater resulting in a reduced α cutoff frequency f_b. This implies more noise at a high bias current. Another low injection effect is that, due to the emitter–base (e–b) junction ideality factor n which becomes as high as 2 at low bias current. These aspects should be incorporated into the bias-dependent noise model for HBTs.

In this paper, thermal effects are included into Hawkins' formula and the obtained results show almost no discrepancy when compared with the experimental measurements. Moreover, the traditional Hawkins' model is slightly modified to include capacitances $C_{\rm De}$ and $C_{\rm bc}$ and their roles in the frequency response of the noise are elaborated in this paper. Associated gain obtained by using the modified noise equivalent circuit is compared with experimental data and shows good agreement.

II. The Model

The noise equivalent circuit is shown in Fig. 1. The circuit is similar to the circuit given by Hawkins except that $C_{\rm De}$ and $C_{\rm bc}$ [8] are included in the present model. The expression for noise figure is derived in Appendix A and is given by

$$F = 1+\frac{r_b}{r_s}+\left(\frac{\overline{i_{cp}^2}}{|\alpha|^2\cdot\overline{e_s^2}}\right)\cdot(A^2+B^2)+\left(\frac{\overline{e_c^2}}{\overline{e_s^2}}\right)\cdot(C^2+D^2) \quad (1)$$

where, A, B, C, and D are given in Appendix A and other notations are explained in Table I. The minimum noise figure $F_{\rm min}$

Manuscript received October 30, 2001; revised May 13, 2002.

M. M. Jahan is with the Intel Corporation, Chandler, AZ 85226 USA.

K.-W. Liu is with the Department of Electronic Engineering, Mingchuan University, Taipei, Taiwan, R.O.C.

A. F. M. Anwar is with the Electrical and Computer Engineering Department, University of Connecticut, Storrs, CT 06269-2157 USA.

Digital Object Identifier 10.1109/TMTT.2003.808699

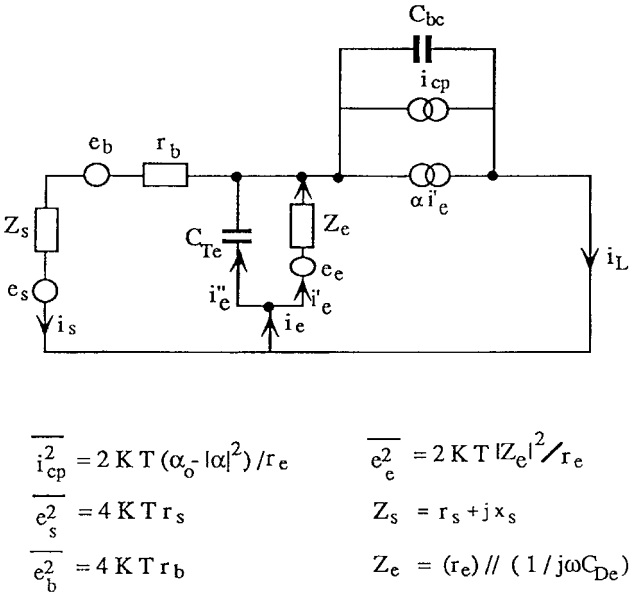

Fig. 1. Modified noise equivalent circuit of an HBT.

may be obtained from (1) by replacing r_s and x_s with the corresponding optimized values [cf. (A16) and (A17)].

At a higher bias (or any bias in general), the junction temperature is different from that of the ambient. For a given collector current, Laplace's equation is solved self-consistently to calculate the junction temperature T. Self-consistent solution is obtained by calculating the junction temperature, for a given collector current, which in turn is used to update the thermal conductivity and the process continues till a consistent solution is obtained. The calculated junction temperature is then used in the determination of the circuit parameters, using updated $\mu_n(T)$, that are used in (1). The temperature distribution across the surface of the chip is calculated by using a temperature simulator routine. The inputs to this routine are the chip dimensions, finger size and location, substrate thermal conductivity, collector voltage, and collector current. The simulator calculates the temperature distribution across the chip based on this information.

By solving the 3-D heat transfer equation $\nabla \cdot \sigma(T) \nabla \cdot T = 0$, the temperature distribution at the surface of the chip can be written as [5] given in (2), shown at the bottom of this page, where

$$C_{0n} = \frac{w}{l}\frac{4 \cdot l_1}{n^2 \cdot \pi^2}\cos\left(\frac{n \cdot \pi}{w} \cdot y_i\right)\sin\left(\frac{n \cdot \pi}{2 \cdot w} \cdot w_i\right) \times \tanh\left(\frac{n \cdot \pi}{w} \cdot d\right) \tag{3}$$

$$C_{m0} = \frac{l}{w}\frac{4 \cdot w_1}{m^2 \cdot \pi^2}\cos\left(\frac{m \cdot \pi}{l} \cdot x_i\right)\sin\left(\frac{m \cdot \pi}{2 \cdot l} \cdot l_i\right) \times \tanh\left(\frac{m \cdot \pi}{l} \cdot d\right) \tag{4}$$

TABLE I

Symbols	Meanings
A_e	emitter area
α	common base current gain
α_0	dc common base current gain
β_0	dc common emitter current gain
C_{Te}	emitter to base depletion capacitance, fF
C_{De}	emitter to base diffusion capacitance, fF
C_{bc}	base to collector depletion capacitance, fF
ΔW	current induced base width increase
ϵ_e	dielectric constant of emitter
ϵ_b	dielectric constant of base
ϵ_c	dielectric constant of collector
f	frequency
f_b	common base current gain cut-off frequency
F_{min}	minimum noise figure, dB
f_T	common emitter unity gain cut-off frequency
I_c	collector current
I_e	emitter current
μ_n	electron mobility
n	emitter-base junction ideality factor
N_{Ab}	base doping concentration
N_{Dc}	collector doping concentration
N_{De}	emitter doping concentration
r_b	intrinsic base resistance, ohm
r_e	emitter-base junction resistance, ohm
r_{opt}	optimum source resistance for minimum noise figure
r_s	source resistance, ohm
t_b	base transit time, sec
v_{eb}	emitter to base voltage
v_{cb}	Collector to base voltage
v_s	saturation velocity
V_{bie}	emitter junction built-in voltage
V_{bic}	collector junction built-in voltage
W	base width
ω_b	$2\pi f_b$
W_c	width of the collector
x_s	source reactance, ohm
x_{opt}	optimum source reactance for minimum noise figure

$$C_{mn} = \frac{16}{mn \cdot \pi^2 \cdot \gamma_{mn}} \cdot \cos\left(\frac{m \cdot \pi}{l} \cdot x_i\right)\cos\left(\frac{n \cdot \pi}{w} \cdot y_i\right) \times \sin\left(\frac{n \cdot \pi}{2 \cdot w} w_i\right)\sin\left(\frac{m \cdot \pi}{2 \cdot l} \cdot l_i\right)\tanh\left(\gamma_{mn} \cdot d\right). \tag{5}$$

Here, N is the total number of the elements, σ is the thermal conductivity, $w(w_i)$ is the width of the chip (ith element), $l(l_i)$ is the length of the chip (ith element), d is the thickness of the chip, and $\gamma_{mn} = \sqrt{(m\pi/l)^2 + (n\pi/w)^2}$. Power density p_i across the ith element is given as

$$p_i = J_{ci} V_{ce} \tag{6}$$

$$T(x,y,0) = \sum_{i=1}^{N}\frac{p_i}{\sigma_i}\left[\sum_{n=1}^{\infty} C_{0n} \cdot \cos\left(\frac{n\pi y}{w}\right) + \sum_{m=1}^{\infty} C_{m0} \cdot \cos\left(\frac{m\pi y}{l}\right) + \sum_{n=1}^{\infty}\sum_{m=1}^{\infty} C_{mn} \cdot \cos\left(\frac{n\pi y}{w}\right)\cos\left(\frac{m\pi y}{l}\right) + \frac{w_i l_i}{wl}\right] \tag{2}$$

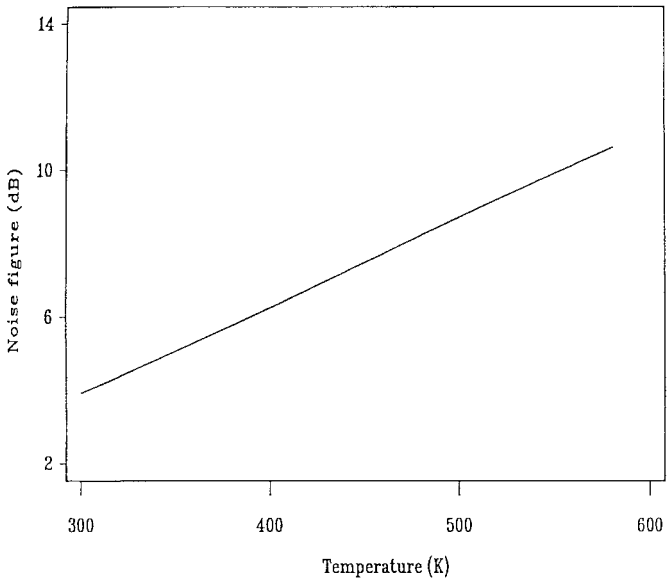

Fig. 2. Noise figure as a function of temperature.

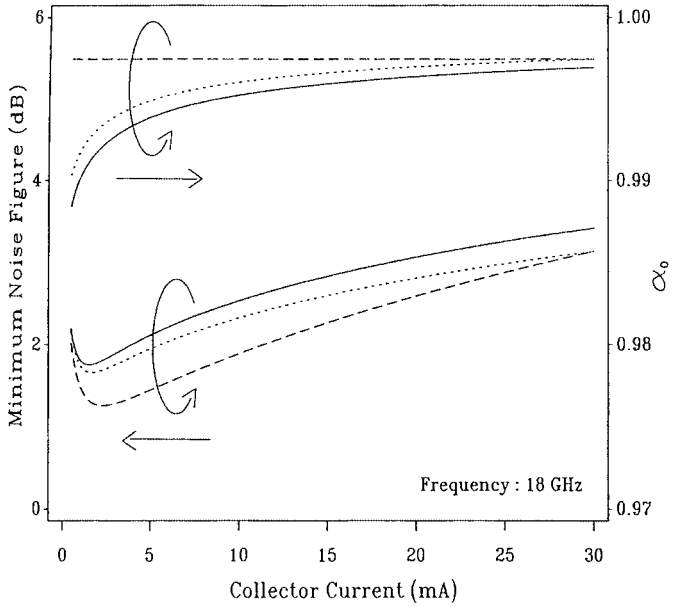

Fig. 3. Effect of bias dependence of α_0 on $F_{\min}$ of an HBT. The solid, dotted, and dashed curves of the top set represent the three different bias dependences of α_0 and correspond to the solid, dotted, and dashed curves, respectively, of the bottom set describing the behavior of $F_{\min}$.

where, J_{ci} is the collector current density at the ith element and V_{ce} is the collector to emitter voltage.

III. Results and Discussions

The important noise sources in the HBTs are: 1) the shot noise due to emitter current; 2) the thermal noise due to base and other parasitic resistances; and 3) the partition noise due to the randomness of the recombination mechanism. Of these, thermal noise varies dramatically with temperature. In order to observe the temperature dependence of the thermal noise, the collector current can be made extremely small, and the noise figure can be calculated for different temperatures. As observed in Fig. 2, under such circumstances, the noise figure increases by around 6 dB for an octave increase (300 K to 600 K) of temperature. This implies almost a T^2 dependence of the thermal noise on the temperature. Although the thermal noise spectral density increases linearly with temperature, the square-of-temperature dependence of the noise figure is due to the resistance which also increases with higher temperature.

The behavior as well as the low bias value of α_0 is crucial in the calculation of $F_{\min}$ and is demonstrated in Fig. 3. $F_{\min}$ becomes greater if α_0 falls off (dotted line) rather than remains constant (dashed line). $F_{\min}$ is also affected by the behavior of the low bias α_0 fall-off. The behavior of α_0 at low bias is similar to that of the homojunction [9], whereas, at high bias current, the decrease of the α_0 is a consequence of base push-out and base–collector space charge width modulation [10]. As evident from Fig. 3, $F_{\min}$ corresponding to smaller α_0 (solid line) at a low bias shows a greater $F_{\min}$. For $I_c = 1$ mA, if the bias dependence of α_0 is assumed to be the solid line, dotted line, and dashed line, respectively, $F_{\min}$ becomes 1.95 dB for the solid line, 1.85 dB for the dotted line, and 1.45 dB for the dashed line. $F_{\min}$ is higher at low values of α_0 at a higher bias. The increased noise at lower α_0 is a consequence of the partition noise source i_{cp} in the equivalent circuit (Fig. 1). The e–b junction ideality factor is also an important parameter that affects low bias noise. The e–b junction leakage current becomes significant at low emitter currents and thus the shot noise contribution at the output is due to the smaller diffusion current that reaches the collector junction, giving a nonunity ideality factor. Fig. 4 shows the plot of $F_{\min}$ versus I_c for different ideality factors. It is observed that $F_{\min}$ at lower bias becomes smaller if $n > 1$ is assumed. $F_{\min}$ at higher bias ($I_c > 4$ mA) remains insensitive to n. Thus, for $n > 1$, low bias noise will be less than that for $n = 1$.

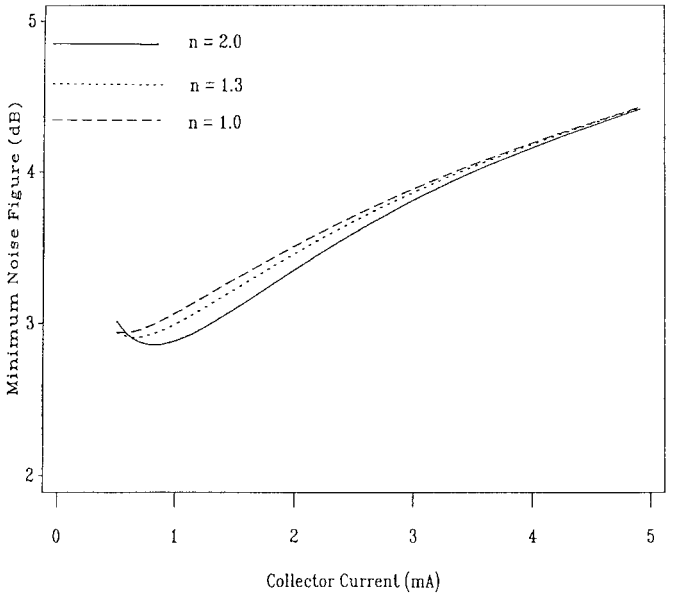

Fig. 4. $F_{\min}$ versus I_c for different n.

The inset of Fig. 5 shows the junction temperature as a function of the collector current for a device with a make-up described in Table II. As the plot suggests, the junction temperature varies significantly from the ambient temperature which

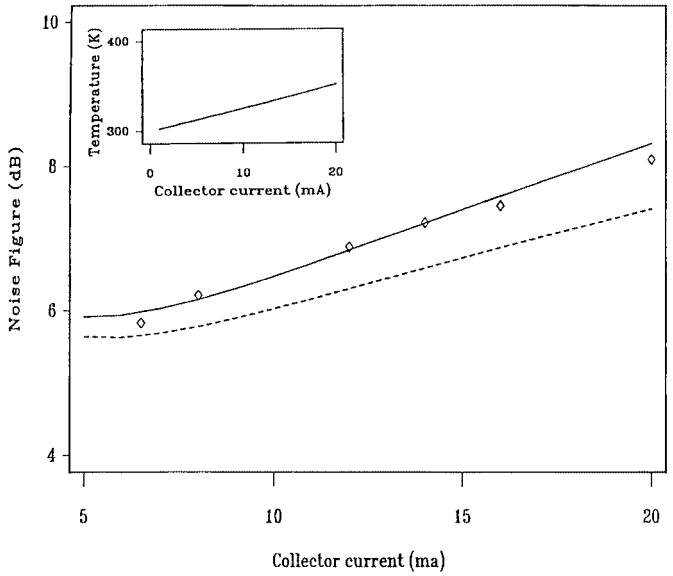

Fig. 5. Comparison of $F_{\min}$ as a function of bias current calculated by using the present model (solid line), the isothermal model (dotted line), and the experimental data (diamond) for a $3.5 \times 3.5\ \mu\text{m}^2$ InP–InGaAs HBT [2] operating at 20 GHz.

demonstrates the need for the inclusion of the actual junction temperature instead of the room temperature in the analysis of the HBTs operated at high junction current. The departure of the actual junction temperature from the isothermal approximation becomes progressively larger as the current increases. The amount of the increase of the junction temperature over the room temperature also depends on the thermal conductivity of the substrate material and the junction area of the device. Since HBTs that are made from III–V compound semiconductors typically have poor thermal conductivity, the rise of the device temperature is rather a serious problem for HBTs. Even SiGe-based HBTs, pursued by several research groups, are not tractable using the isothermal model at high bias. Moreover, as the device junction area has to be substantially scaled down for microwave applications, the increased junction temperature is even more critical for microwave HBTs, and the feasibility of using techniques such as thermal shunts may be investigated.

Fig. 5 shows the plot of noise figure versus collector current for the HBT [2] with the device make-up given in Table II. For comparison, the experimental results (diamond), the isothermal calculation (dotted line), and the present calculation (solid line) have all been shown on the same plot. As is apparent, the discrepancies exist between the experimental measurement and the isothermal calculation. The present calculation, where the effect of the actual junction heating as a function of bias current is included, shows a close agreement with the experimentally measured values. In Fig. 6, calculated $F_{\min}$ (solid lines) is plotted as a function of frequency over a range of 2–18 GHz for the same device. The excellent fit between the theoretical calculation and the measured data are again due to the inclusion of the bias-dependent junction heating as well as C_{De} and C_{bc} into the present calculation. The contribution of C_{De} is found to be even more important at high frequencies, contrary to the common belief that it becomes insignificant at that frequency (see Appendix A). The role of C_{bc} is to reduce the noise by establishing a negative

TABLE II
PARAMETERS USED IN THE SIMULATION [2], [5]

Parameters	Expression
InP emitter	2500 Å($n = 1 \times 10^{18}\ cm^{-3}$)
$InGaAs$ base	500Å ($p = 1 \times 10^{20}\ cm^3$)
$InGaAs$ collector	3000 Å($n = 2 \times 10^{16}$)
InP substrate	$100\mu m$
e-b junction capacitance (C_{je})	$220fF$
c-b junction capacitance (C_{bc})	$21fF$
Emitter junction area	$3.5 \times 3.5\ \mu^2$
Base resistance	120Ω (at 300 K)
$\sigma(T)$	$0.76 - 0.001 \cdot T$
$\mu_n(T)$	$7200/((1 + 5.5 \times 10^{-17} \cdot n_{a0}^{0.233}) \cdot (300/T)^{2.3}$
Ideality factor n	1
Frequency f	20GHz

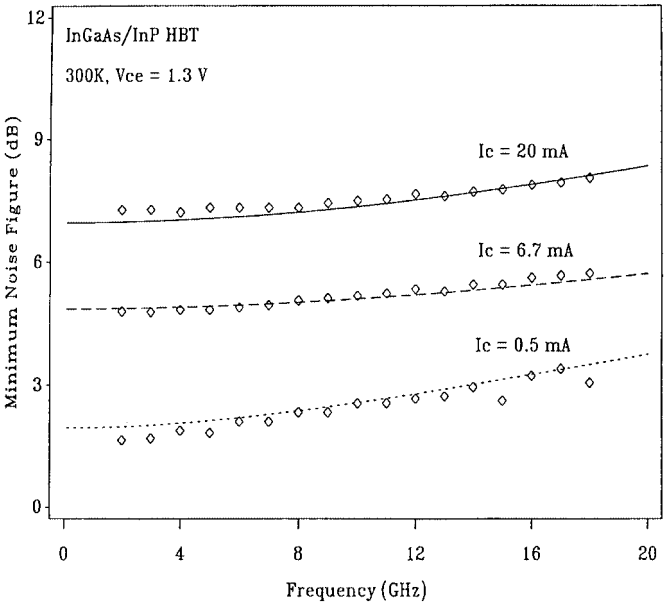

Fig. 6. Comparison of $F_{\min}$ as a function of frequency calculated by using the present model (solid line) and the experimental data (diamonds) for a $3.5 \times 3.5\ \mu\text{m}^2$ InP–InGaAs HBT at 300 K [2].

feedback from the output to the input. The presence of C_{bc} in the noise-equivalent circuit will reduce noise, as is evident from (A8). However, if a measurement of minimum noise figure is made, the effect of C_{bc} is minimal. This may be explained by the fact that C_{bc} reduces both noise and associated gain, making $F_{\min}$ insensitive to any variation of C_{bc}. Therefore, the negelect of C_{bc} in the noise-equivalent circuit is permissible for $F_{\min}$ (in the limit $r_b \ll r_s, x_s$) measurement, however, an independent measurement of noise necessitates the incorporation of the negative feedback due to C_{bc}. Fig. 7 shows the calculated associated gain as a function of frequency for a collector current of 0.3 mA with $V_{\text{ce}} = 1.3$ V [2]. On the same plot, experimental data are shown to demonstrate good agreement. Associated gain is formulated as

$$G = \frac{1 - |\Gamma_s|^2}{|1 - s_{11}\Gamma_s|^2}|s_{21}|^2 \tag{7}$$

where Γ_s is the source reflection coefficient. A termination of 50 Ω is assumed throughout the analysis. The gain calculation

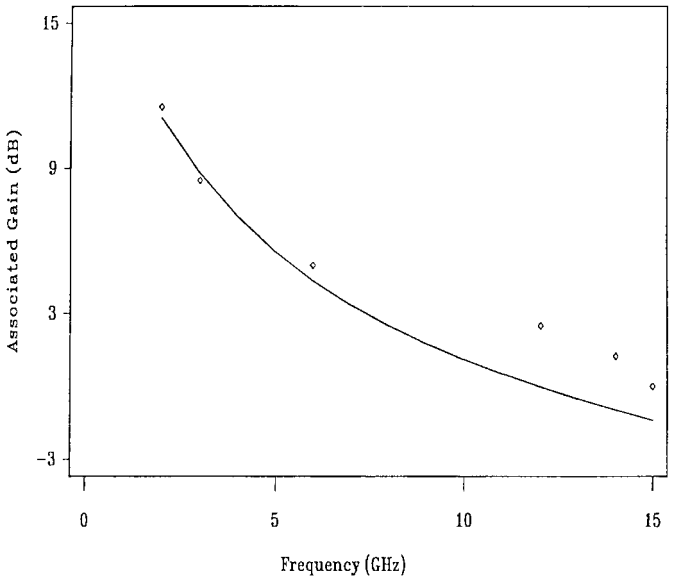

Fig. 7. Comparison of associated gain at $I_c = 0.3$ mA (solid line: present calculation; diamonds: measured data [2]).

follows the derivation presented in Appendix B. The calculations are performed by assuming an optmimized input and reflectionless load termination. The optimized source impedance is the same as that used for the evaluation of a minimum noise figure.

IV. Conclusion

The need for the inclusion of the bias dependence of different transistor parameters into the high-frequency noise formulation has been emphasized in this paper. An expression for $F_{\min}$ is derived by taking the bias dependence of the transistor parameters (i.e., $C_{\rm De}$, $C_{\rm bc}$) into account. The junction heating, which becomes important at higher collector currents, is also incorporated into the analysis of the high-frequency noise figure calculation. It is observed that the estimation of noise figure based on the isothermal calculation underestimates the device noise at higher bias current. The inclusion of the junction heating effect into the noise figure calculation yields an excellent fit to the experimental results. As far as the emitter size is concerned, there exists a tradeoff between the noise performance and the speed of the device. These issues together with the particular aspect of noise enhancement should be given very careful thought before designing a microwave HBT device for high-frequency communication circuitry.

Appendix A

Referring to Fig. 1, applying KVL at the input, one obtains

$$e_s + e_e + e_b = i_s \cdot Z_s + i'_e \cdot Z_e + i_s \cdot r_b \tag{A1}$$

where $Z_s = r_s + jx_s$ and $Z_e = r_e \parallel (1/j\omega C_{\rm De})$. $C_{\rm De}$ and r_e can be obtained from the imaginary and real parts of the admittance as [9]$Y = G_d + j\cdot\omega\cdot C_{\rm De}$. At low frequencies ($\omega \ll 1/\tau_n$, $\omega\tau_n \ll 1$), one obtains $G_{d0} = q\cdot\mu_n(T)\cdot(n_{b0}/L_n)e^{qV_{\rm bc}/kT}$ and $C_{\rm De0} = q\cdot\mu_n(T)\cdot(n_{b0}/L_n)\tau_n\cdot e^{qV_{\rm bc}/kT}$ and $Y = G_{d0}(1 + j\cdot\omega\cdot\tau_n) \sim G_{d0} = 1/r_e$ and the contribution of the reactive branch seems to be minimal. Therefore, $C_{\rm De0}$ does not play a major role in circuit performance at low frequencies. At high frequencies, however, we have

$$G_d = G_{d0}\cdot\tau_n\omega^{1/2} \tag{A2}$$

and

$$C_{\rm De} = C_{De0}\tau_n\omega^{1/2}. \tag{A3}$$

Therefore, contrary to the common belief, minimal $C_{\rm De}$ contribution at high frequencies cannot be justified and the admittance should be expressed as $Y = G_d(1+j)$. Following the treatment of Anderson [11], the emitter-to-base depletion region capacitance $C_{\rm Te}$ and $C_{\rm bc}$ are given as

$$C_{\rm Te} = \sqrt{\frac{qN_{\rm De}N_{\rm Ab}\epsilon_e\epsilon_b}{2(\epsilon_e N_{\rm De} + \epsilon_b N_{\rm Ab})(V_{bie} - v_{\rm eb})}} \tag{A4}$$

and

$$C_{\rm bc} = \sqrt{\frac{qN_{\rm Dc}N_{Ab}\epsilon_c\epsilon_b}{2(\epsilon_c N_{\rm Dc} + \epsilon_b N_{\rm Ab})(V_{\rm bic} + v_{\rm cb})}}. \tag{A5}$$

Applying KCL, i_L and i_e may be written as

$$i_L = \alpha\cdot i'_e + i_{\rm cp} + i_{\rm bc} \tag{A6}$$

$$i_e = i'_e + i''_e. \tag{A7}$$

After simplification, i_L is then defined as given in (A8), shown at the bottom of this page. Noise figure is defined as the ratio

$$i_L = \frac{e_s + e_b + \dfrac{i_{\rm cp}}{\alpha}\cdot\left[\left(\dfrac{\alpha}{\alpha - j\cdot\omega C_{\rm bc}Z_e} + j\cdot\omega\cdot C_{\rm Te}\cdot Z_e\right)\cdot(Z_s + r_b) + \dfrac{\alpha}{\alpha - j\cdot\omega\cdot C_{\rm bc}\cdot Z_e}\cdot Z_e\right]}{\dfrac{1}{\alpha}\cdot\left[\dfrac{j\cdot\omega\cdot C_{\rm bc}Z_e}{\alpha - j\cdot\omega\cdot C_{\rm bc}\cdot Z_e}\cdot(Z_s + r_b + Z_e) + (1 + j\cdot\omega\cdot C_{\rm Te}\cdot Z_e)\cdot(Z_s + r_b) + Z_e\right]}$$
$$+\frac{e_e\cdot\left[\left(\dfrac{j\cdot\omega\cdot C_{\rm bc}}{\alpha - j\cdot\omega\cdot C_{\rm bc}\cdot Z_e} + j\cdot\omega\cdot C_{\rm Te}\right)\cdot(Z_s + r_b) + \dfrac{\alpha}{\alpha - j\cdot\omega\cdot C_{\rm bc}\cdot Z_e}\cdot Z_e\right]}{\dfrac{1}{\alpha}\cdot\left[\dfrac{j\cdot\omega\cdot C_{bc}Z_e}{\alpha - j\cdot\omega\cdot C_{bc}\cdot Z_e}\cdot(Z_s + r_b + Z_e) + (1 + j\cdot\omega\cdot C_{\rm Te}\cdot Z_e)\cdot(Z_s + r_b) + Z_e\right]} \tag{A8}$$

of the output noise power to that from a noiseless but otherwise identical device, i.e.,

$$F = \frac{\overline{i_L^2}}{\overline{i_{L0}^2}} \tag{A9}$$

where i_{L0} is the value of i_L due to the source generator e_s alone (e_e, e_b, and i_{cp} equal to zero). The noise figure can now be expressed as

$$F = 1 + \frac{r_b}{r_s} + \left(\frac{\overline{i_{\rm cp}^2}}{|\alpha|^2 \cdot \overline{e_s^2}}\right) \cdot (A^2 + B^2) + \left(\frac{\overline{e_e^2}}{\overline{e_s^2}}\right) \cdot (C^2 + D^2) \tag{A10}$$

where

$$\begin{aligned} A =& (r_s + r_b + R_e) \cdot R_m - X_m \cdot (x_s - X_e) \\ &+ (r_s + r_b)(\omega \cdot X_e \cdot C_{\rm Te}) - x_s \cdot \omega \cdot R_e \cdot C_{\rm te} \end{aligned} \tag{A11}$$

$$\begin{aligned} B =& R_m \cdot (x_s - X_e) + X_m \cdot (r_s + r_b + R_e) \\ &+ \omega \cdot R_e \cdot C_{\rm Te} \cdot (r_s + r_b) + x_s \cdot \omega \cdot X_e \cdot C_{\rm Te} \end{aligned} \tag{A12}$$

$$C = R_m - \omega \cdot C_{Te} \cdot x_s - (r_s + r_b) \cdot \frac{\omega \cdot C_{\rm bc} \cdot X_m}{|\alpha|} \tag{A13}$$

$$D = (r_s + r_b) \cdot \omega \cdot C_{\rm Te} + \frac{\omega \cdot C_{\rm bc}}{|\alpha|} \cdot X_m \cdot x_s + X_m \tag{A14}$$

and R_m and X_m are the real and imaginary parts, respectively, of the following quantity:

$$\frac{\alpha_R + j \cdot \alpha_I}{(\alpha_R - \omega \cdot C_{\rm bc} \cdot X_e) + j \cdot (\alpha_I - \omega \cdot C_{\rm bc} \cdot X_e)} \tag{A15}$$

where α_R and α_I are the real and imaginary parts of α.

Optimizing noise figure with respect to source resistance r_s and source reactance x_s, one can find the optimum source resistance $R_{\rm opt}$ and optimum source reactance $X_{\rm opt}$ as given in (A16) and (A17), shown at the bottom of this page, where

$$\begin{aligned} A_1 =& \frac{|Z_e|}{2}(T_1^2 + T_2^2) + \frac{\alpha_0 - |\alpha|^2}{2|\alpha|^2|Z_e|}(P_1^2 + P_2^2) \\ C_1 =& -\frac{|Z_e|}{2}(T_3^2 + T_4^2) - \frac{\alpha_0 - |\alpha|^2}{2|\alpha|^2|Z_e|}(Q_1^2 + Q_2^2) \\ T_1 =& -\frac{\omega \cdot C_{\rm bc} \cdot X_m}{\alpha} \\ T_2 =& \omega \cdot C_{Te} \\ T_3 =& R_m \left(1 - \frac{\omega \cdot C_{\rm bc} \cdot X_m}{\alpha}\right) - \omega \cdot C_{\rm Te} \cdot x_s \\ T_4 =& r_b \cdot \omega C_{\rm Te} + X_m - \frac{x_s \cdot X_m \cdot \omega \cdot C_{\rm bc}}{\alpha} \end{aligned}$$

$$\begin{aligned} P_1 =& \omega \cdot X_e \cdot C_{Te} + R_m \\ P_2 =& \omega \cdot R_e \cdot C_{\rm Te} + X_m \\ Q_1 =& -x_s(X_m + \omega \cdot R_e \cdot C_{\rm Te}) \\ &+ R_m(r_b + R_e) + X_m \cdot X_e + r_b \cdot \omega \cdot X_e \cdot C_{\rm Te} \\ Q_2 =& -r_b \cdot \omega \cdot R_e \cdot C_{\rm Te} + R_m(X_e - x_s) \\ &- X_m(r_b + R_e + \omega \cdot C_{\rm Te} \cdot X_e) \\ Z_e =& R_e + jX_e. \end{aligned}$$

APPENDIX B

The formulation of the minimum noise figure may be expressed as the ratio of the input to output noise and the reciprocal of the associated gain. Thus, the associated gain calculation is desirable which not only can be used to verify the measured noise figure data but also can be used to model different small-signal parameters of the equivalent circuit. In the following, the associated gain is calculated in terms of s parameters. The four scattering parameters (s_{11}, s_{21}, s_{12}, s_{22}), based on the circuit shown in Fig. 1, are expressed in terms of the Y-parameters as follows:

$$\begin{aligned} s_{11} =& \frac{(1 - y_{11})(1 + y_{22}) + y_{12} \times y_{21}}{\Delta} \\ s_{12} =& -2\frac{y_{12}}{\Delta} \\ s21 =& -2\frac{y_{21}}{\Delta} \\ s22 =& \frac{(1 + y_{11})(1 - y_{22}) + y_{12} * y_{21}}{\Delta} \end{aligned} \tag{B1}$$

where

$$\begin{aligned} \Delta =& (1 + y_{11})(1 + y_{22}) - y_{12}y_{21} \\ y_{11} =& \frac{s \cdot r_e \cdot C_e + 1 - \alpha + s \cdot r_e \cdot C_{\rm bc}}{r_e + r_b(s \cdot r_e \cdot C_e + 1 - \alpha + s \cdot r_e \cdot C_{\rm bc}} \\ y_{22} =& \frac{r_e + r_b + s \cdot C_e \cdot r_e \cdot r_b)s \cdot C_{\rm bc}}{s \cdot c_{\rm bc} \cdot r_e \cdot r_b + r_e + r_b + s \cdot r_b \cdot r_e \cdot c_e - \alpha \cdot r_b} \\ y_{21} =& -\frac{s \cdot r_e \cdot C_{\rm bc} - \alpha}{r_e + r_b(s \cdot r_e \cdot C_e + 1 - \alpha + s \cdot r_e \cdot C_{\rm bc}} \\ y_{12} =& \frac{s \cdot r_e \cdot C_{\rm bc}}{s \cdot C_{\rm bc} \cdot r_e \cdot r_b + r_e + r_b + s \cdot r_b \cdot r_e \cdot C_e - \alpha \cdot r_b} \end{aligned} \tag{B2}$$

with $s = j \cdot 2 \cdot \pi \cdot f$.

$$X_{\rm opt} = \frac{\frac{1}{|\alpha|} \cdot \left(\frac{\alpha_0}{|\alpha|^2} - 1\right) \cdot (R_m^2 + X_m^2) \cdot X_e + |Z_e| \cdot \omega \cdot \left(\frac{\alpha_0}{|\alpha|^2} \cdot R_m \cdot C_{\rm Te} + \frac{C_{\rm bc}}{|\alpha|} \cdot X_m^2\right)}{\frac{1}{|\alpha|}\left(\frac{\alpha_0}{|\alpha|^2} - 1\right)(R_m^2 + X_m^2) + 2\omega C_{\rm Te}(R_e X_m + R_m X_e) + \frac{\omega^2 |Z_e|}{|\alpha|^2}(\alpha_0 C_{\rm Te}^2 + X_m^2 C_{\rm bc}^2)} \tag{A16}$$

$$R_{\rm opt} = \sqrt{-\frac{C_1}{A_1}} \tag{A17}$$

The gain is computed as

$$G = \frac{1 - |\Gamma_s|^2}{|1 - s_{11}\Gamma_s|^2}|s_{21}|^2 \tag{B3}$$

where Γ_s is the source reflection coefficient. A termination of 50 Ω is assumed throughout the analysis.

REFERENCES

[1] R. J. Hawkins, "Limitations of Nielsen's and related noise equations applied to microwave bipolar transistors, and a new expression for the frequency and current dependent noise figure," *Solid State Electron.*, vol. 20, pp. 191–196, 1977.

[2] Y. Chen, R. N. Nottenburg, M. R. Panish, R. A. Hamm, and D. A. Humphrey, "Microwave noise performance of InP/InGaAs heterostructure bipolar transistors," *IEEE Electron Device Lett.*, vol. 10, pp. 470–472, Oct. 1989.

[3] H. Schumacher, U. Erben, and A. Gruhle, "Noise characteristics of Si/SiGe heterojunction bipolar transistors at microwave frequencies," *Electron. Lett.*, vol. 28, pp. 1167–1168, 1992.

[4] L. Escotte, J. G. Tartarin, R. Plant, and J. Graffeuil, "High-frequency noise in heterojunction bipolar transistors," *Solid State Electron.*, vol. 42, pp. 661–663, 1998.

[5] G.-B. Gao, M.-Z. Wang, X. Gui, and H. Markoc, "Thermal design studies of high-power heterojunction bipolar transistors," *IEEE Trans. Electron Devices*, vol. 36, pp. 854–863, May 1989.

[6] C.-W. Kim, N. Goto, and K. Honjo, "Thermal behavior depending on emitter finger and substrate configurations in power heterojunction bipolar transistors," *IEEE Trans. Electron Devices*, vol. 45, pp. 1190–1195, June 1998.

[7] J. J. Liou, L. L. Liou, C. I. Huang, and B. Bayraktaroglu, "A physics-based, analytical heterojunction bipolar transistor model including thermal and high-current effects," *IEEE Trans. Electron Devices*, vol. 40, pp. 1570–1577, Sept. 1993.

[8] H. F. Cooke, "Microwave transistors: Theory and design," *Proc. IRE*, vol. 59, pp. 1163–1181, 1971.

[9] S. M. Sze, *Physics of Semiconductor Devices*, 2nd ed. New York: Wiley, 1981.

[10] B. R. Ryum and I. M. Abdel-Motaleb, "A Gummel-Poon model for abrupt and graded heterojunction bipolar transistors (HBT's)," *Solid State Electron.*, vol. 33, pp. 869–880, 1990.

[11] R. L. Anderson, "Experiments on Ge–GaAs heterojunction," *Solid State Electron.*, vol. 5, pp. 341–351, 1962.

Mirza M. Jahan was born in Dhaka, Bangladesh, on January 21, 1966. He received the B.S. degree in electrical engineering from the Bangladesh University of Engineering and Technology, Dhaka, Bangladesh, in 1989, and the M.S. and Ph.D. degrees from the University of Connecticut, Storrs, in 1992 and 1995, respectively.

In 1995, he joined the Intel Corporation, Chandler, AZ, and since then has been engaged in designing PentiumPro, Pentium III, Xeon, and Pentium IV microprocessors by leading the I/O Design Team, Package Design Team, Reliability Verification Team, and Low-Power Team. He is currently leading the standard Cell Design Team for Intel's wireless product line and driving the ultralow-power intitiative for the deep-submicrometer design. He has authored/coauthored and presented many papers in different journals and conferences. He has also filed patents on high-speed circuit design.

Kuo-Wei Liu received the B.S. degree from the National Taiwan Ocean University, Taiwan, R.O.C., in 1982, the M.S. degree from Syracuse University, Syracuse, NY, in 1990, and the Ph.D. degree from the University of Connecticut, Storrs, in 1994.

He is currently an Associate Professor and Department Head with the Department of Electronic Engineering, Mingchuan University, Taipei, Taiwan, R.O.C. His current research interests are in the areas of noise study of microelectronics (HEMTs, HBTs), and optoelectronics.

A. F. M. Anwar (S'86–M'88–SM'00) received the B.S. and M.S. degrees in electrical and electronic engineering from the Bangladesh University of Engineering and Technology (BUET), Dhaka, Bangladesh, in 1982 and 1984, respectively, and the Ph.D. degree from Clarkson University, Potsdam, NY, in 1988.

He is currently a Professor with the Department of Electrical and Computer Engineering, University of Connecticut, Storrs. His research group, in the RF Microelectronics and Noise Laboratory, is currently involved in the study of transport in short heterostructures and antimony-based HEMTs operating above 300 GHz. Moreover, the group is involved in modeling GaN-based high-power HEMTs and HBTs. He is also active in research in the areas of CMOS-based class-E amplifiers, as well as transport dynamics and noise in resonant tunneling diodes and one-dimensional structures.

Dr. Anwar is an editor for the IEEE TRANSACTIONS ON ELECTRON DEVICES.